Cancer Immunology, Immunotherapy (2025) 74:128
https://doi.org/10.1007/s00262-025-03983-8

RESEARCH

Single-cell transcriptome sequencing reveals the immune microenvironment in bronchoalveolar lavage fluid of checkpoint inhibitor-related pneumonitis

Linpeng Zheng[1] · Fenglin Lin[1] · Dingqin Cai[1,2] · Longyao Zhang[1] · Chenrui Yin[1] · Yaxian Qi[1] · Lingyou Sun[1] · Lingchen Li[1] · Xiewan Chen[1,3] · Jianbo Zhu[1] · Jianguo Sun[1]

Received: 16 October 2024 / Accepted: 17 February 2025 / Published online: 1 March 2025

Abstract

Background and objectives Immune checkpoint inhibitors (ICIs) bring cancer patients tumor control and survival benefits, yet they also trigger immune-related adverse effects (irAEs), notably checkpoint inhibitor-related pneumonitis (CIP), affecting about 5% of patients among whom 1–2% experiencing severe grade 3 or higher pneumonitis. Current research points to potential links with T cell subset dysfunction and autoantibody increase, but the specific mechanisms underlying different grades of CIP are understudied.

Methods Herein, we employed single-cell RNA sequencing (scRNA-seq) on bronchoalveolar lavage fluid (BALF) from CIP patients across varying severity levels, aiming to elucidate underlying immune environment and mechanisms of CIP progression at cellular and molecular levels.

Findings Totally, 121,409 high qualified cells from BALF of 11 patients were annotated and categorized into five major cell types. Severe CIP (CIP-S) cases have a significant increase in the percentage of unreported epithelial cells in their bronchoalveolar lavage fluid compared with mild CIP (CIP-M) cases. These cells were defined as aberrant basaloid cells. They upregulated SOX9, increased the expression of CXCL3/5, recruited neutrophils, and activated the immune system. Additionally, macrophages in the CIP-S group had stronger antigen-presenting abilities and resulted in more CD8 + effective T cells infiltrated.

Conclusions Utilizing single-cell sequencing of BALF, we discovered an enriched population of aberrant basaloid cells in CIP-S patients, which had not been previously reported. Aberrant basaloid cells may upregulate SOX9 via CXCL3/5-CXCR2 to recruit and activate neutrophils, and further activate the immune system, resulting in CIP-S. This finding could identify new targets for stratified treatment of CIP patients, holding promise of a novel approach for clinical guidance.

Keywords Checkpoint inhibitor-related pneumonitis · Single-cell RNA sequencing · Aberrant basaloid cell · Neutrophil · T cell · Macrophage

Introduction

Immune checkpoint inhibitors (ICIs) bring both tumor control and survival advantages to cancer patients, but they also result in immune-related adverse effects (irAEs) [24]. One of the common side effects is checkpoint inhibitor-related pneumonitis (CIP), which has a total incidence rate of about 5% and a rate of 1–2% for grade 3 or higher pneumonitis [12, 14]. Current research indicates that CIP may be associated with T cell subsets dysfunction, increase in existing and new autoantibodies, programmed death ligand 2 (PD-L2), and so forth [5, 20, 32, 33]. However, few studies focus on the specific mechanisms of different grades of CIP. Bronchoalveolar

✉ Jianguo Sun
sunjianguo@tmmu.edu.cn

1 Cancer Institute, Xinqiao Hospital, Army Medical University, Chongqing, China

2 921, Hospital of PLA (Second Affiliated Hospital of Hunan Normal University), Changsha, China

3 Department of Basic Medicine, Army Medical University, Chongqing, China

lavage fluid (BALF) in respiratory diseases, particularly lower airway diseases, is important for diagnosis, efficacy observation, prognosis judgment, and pathogenesis study [6, 29, 34, 39]. Single-cell sequencing technology can reveal the genetic structure and gene expression state of individual cells, reflecting the heterogeneity that cannot be obtained from the mixed samples sequenced, and thereby is used to explore the occurrence and development of diseases at a more microscopic, direct, and precise level [11, 18, 26, 42, 42, 43, 43].

Herein, we collected BALF from CIP patients at different grades and performed single-cell RNA sequencing (scRNA-Seq) to uncover the underlying mechanisms among the various stages of CIP.

Methods

Patient cohort and characteristics

This study had been registered at ClinicalTrials.gov. (NCT05455034) and received ethical approval from the hospital (NO. 2022-022-01). Patients who were diagnosed with CIP and consenting to a BALF procedure from March. 1, 2023 to May 31, 2024 were enrolled into this study in the Department of Oncology at Xinqiao Hospital. All of them were diagnosed according to the Management of Immune Checkpoint inhibitor-related Toxicity Guidelines published by Chinese Society of Clinical Oncology, 2023 (CSCO). The main diagnostic criteria include: having a history of ICIs use; newly appeared pulmonary shadows, such as ground—glass opacities, patchy consolidation shadows, interlobular septal thickening, reticular shadows, traction bronchiectasis, and fibrous streak shadows; excluding pulmonary infections, progression of pulmonary tumors, interstitial lung diseases caused by other reasons, pulmonary vasculitis, pulmonary embolism, and pulmonary edema, etc. Symptom grading is based on the $r =$ following criteria. Grade1: Asymptomatic; limited to 1 lobe or $< 25\%$ lung parenchyma. Grade2: New or worsened symptoms (e.g., dyspnea, cough, chest pain, fever, hypoxia); multiple lobes involved (25–50% parenchyma), impacts daily life, needs drug treatment. Grade3: Severe symptoms, all lobes or $> 50\%$ parenchyma affected, self-care limited, hospitalization needed. Grade4: Life-threatening dyspnea, ARDS, requires emergency intubation. Exclusion criteria included having any diseases requiring systemic corticosteroids or other immunosuppressive drugs for treatment within 14 days before enrollment, experiencing serious infection, including but not limited to complications of infection, bacteremia, or severe pneumonia, resulting in hospitalization for treatment within 4 weeks before enrollment, or receiving any other investigational drug treatments or participating in other clinical trials within 4 weeks before enrollment. Grades 3 and 4 were classified as severe CIP (CIP-S) group and Grades 1 and 2 were assigned to mild CIP (CIP-M) group. More detailed cohort characteristics are shown in Table 1.

Bronchoalveolar lavage fluid collection

The lung segment underwent local anesthesia, and then the bronchoscope tip was inserted into the opening of the lobule or sub-lobule. Sterile saline at 37 °C was rapidly injected, usually 25 to 50 ml each time, totaling 100 to 250 ml, and immediate aspiration recovery of the wash liquid was realized using a pressure of 50 to 100 mmHg, which is typically about 50% recovered. About 30 ml of lavage fluid from the lung lobe, where pneumonia occurred will be collected from each patient. Subsequently, BALF is promptly put into an ice-filled foam box for brief preservation.

Single-cell RNA sequencing and preprocessing data

BALF was filtered through a 70-micron cell strainer, and red blood cells were lysed. Trypan blue was used to assess cell viability, and then cell concentration was adjusted to 2×10^5 cells/mL before withdrawing 100 µl for Singleron Matrix® Single-Cell Processing System. Following extraction from a microwell chip, barcoded beads facilitated the reverse transcription of captured mRNA into cDNA, which was amplified via PCR. Fragmented and adapter-ligated cDNA formed scRNA-seq libraries per the GEXSCOPE® protocol [10]. After being diluted to 4 nM and pooled, these libraries were sequenced on an Illumina Novaseq 6000, yielding 150 bp paired-end reads for cellular and expression analyses.

Table 1 Characteristics of patient cohorts for scRNA - seq analysis

	CIP-S ($n=4$)	CIP-M ($n=7$)
Sex		
Men	4 (100%)	6 (85.7%)
Women	0	1 (14.3%)
Age	70.8	64.1
Smoking history		
Former	3 (75%)	5 (71.4%)
Never	1 (25%)	2 (28.6%)
COPD	0	0
ICIs		
Pembrolizumab	2 (50%)	2 (28.6%)
Toripalimab	1 (25%)	3 (42.9%)
Duralumab	1 (25%)	1 (14.3%)
Tislelizumab	0	1 (14.3%)
Prior thoracic radiotherapy	1 (25%)	4 (57.1%)
Median time from treatment to CIP	249.5	290.4
Median time from CIP to OS	58.5	NA

Using CeleScope (version 1.9.0), available at https://github.com/singleron-RD/CeleScope, the initial transcriptomic data obtained from scRNA-seq was refined to create matrices of gene expression. In summary, the process involved preprocessing the raw reads through CeleScope to eliminate low-quality sequences, which included using Cutadapt (V1.17) to trim both poly-A tails and adapter remnants. Subsequently, the cell barcode and Unique Molecular Identifiers (UMIs) were isolated. Following this, STAR (V2.6.1a) was employed to align the reads to the reference genome GRCh38 (hg38), specifically the Ensembl version 92 annotation [8]. The quantification of UMIs and genes within each cell was achieved via the application of featureCounts (V2.0.1), culminating in the formation of expression matrix that were further used for downstream analyses [22].

Quality control, dimension-reduction and clustering

Using Scanpy v1.8.1 and Python 3.7, we conducted quality control, dimensionality reduction, and clustering on sample datasets [37]. After filtering out cells with low gene counts (< 200), high UMI counts (top 2%), excessive mitochondrial content (> 50%), and poorly expressed genes (< 5), we retained 121,409 cells. Normalization, selection of variable genes, and PCA were followed by batch effect removal [38]. Cells were clustered into 20 groups via Louvain algorithm with a resolution parameter of 1.2 and visualized using Uniform Manifold Approximation and Projection (UMAP).

Differentially expressed genes (DEGs) and pathway enrichment analyses

Using scanpy's rank genes groups, we identified DEGs via Wilcoxon rank-sum tests. Criteria included expression in > 10% cells, mean log (FC) > 0.25, and Benjamini–Hochberg correction p value < 0.05.

To investigate gene functions, GO and KEGG assessments were conducted using the "clusterProfiler" R package v3.16.1 [31]. Pathways with an adjusted p-value under 0.05 were marked as significantly enriched. GSEA was performed in Neutrophils clusters.

Cell–cell interaction analysis (CellChat and CellPhoneDB)

The CellChat software with a version number of 0.0.2 was employed for examining the networks of cellular interactions derived from scRNA-Seq data[17]. An instance of CellChat was established through the utilization of the R package's processing capabilities. Information about cells was incorporated into the metadata section of this instance. Subsequently, the database containing information on ligand-receptor interactions was configured, and calculations to infer receptor associations were executed.

When it comes to CellPhoneDB, permutation number for calculating the null distribution of average ligand-receptor pair expression in randomized cell identities was set to 1000. Ligand or receptor expression for individual genes was thresholded by using a cutoff derived from the average log gene expression across all genes for each cell type. Predicted interaction pairs with p value < 0.05 and of average log expression > 0.1 were considered as significant and visualized by heatmap plot and dot plot in CellphoneDB.

UCell gene set scoring

Gene set scoring was performed using the *R* package UCell v 1.1.0[3]. UCell scores were based on the Mann–Whitney U statistic by ranking query genes in order of their expression levels in individual cells.

Statistical analysis

To measure cell distribution in clusters, we used the Observed to Expected Ratio (Ro/e), calculated as Observed/Expected, with values > 1 signifying enrichment in the group. Observed is actual cell count, and expected is chi-square predicted count [41].

CNV

The InferCNV package [35] was used to detect the CNAs in aberrant basaloid cells. Lymphocytes cells were used as baselines to estimate the CNAs of malignant cells. Genes expressed in more than 20 cells were sorted based on their loci on each chromosome. The relative expression values were centered to 1, using 1.5 standard deviation from the residual-normalized expression values as the floor and ceiling. A slide window size of 101 genes was used to smoothen the relative expression on each chromosome, to remove the effect of gene-specific expression. The inferred CNAs on each short or long arm or full length of the chromosomes were visualized with heatmaps generated by *R*p heatmap function. The clonal relationships of malignant cell clusters in each sample were determined by the accumulation of CNAs. The CNV score of each cell was calculated as quadratic sum of CNA region.

Flow cytometry

In order to verify our results, the following flow cytometry antibodies were employed. MIEN1 Antibody (PE, NBP2-74899PE, Novus), MMP-7 (AF647, sc-515703AF647, SantaCruz), ERBB2 (AF488, 324,410, BioLegend), CD45 (Pacific Blue, 304,022, BioLegend), CD14 (FITC, 301,804,

BioLegend), CD16 (PE-Cy7, 557,744, BD Pharmingen), CD24 (BB700, 566,524, BD Pharmingen), CD206 (PE, 321,105, BioLegend), CD68 (AF488, 333,811, BioLegend), CD3 (PO, CD0330TR, Thermo), CD8(PE-Cy7, 557,746, BD Pharmingen), CD4 (Percp-cy5.5, 300,530, BioLegend), L/D (FVS780, 565,388, BioLegend), Fixation and Permeablization Kit (554,714, BD Pharmingen). Detected by Beckman coulter (Gallios) and analyzed by FlowJo software (Version10.8.1).

Results

Main cell types of CIP in BALF

We collected BALF from 11 donors, including four CIP-S and seven CIP-M patients (Fig. 1a). The median age was 70.8 years in CIP-S group and 64.1 in CIP-M. In the CIP-S group, two patients were diagnosed with lung cancer, one was esophageal cancer, one was laryngeal cancer, three patients had a history of smoking, two used Pembrolizumab,

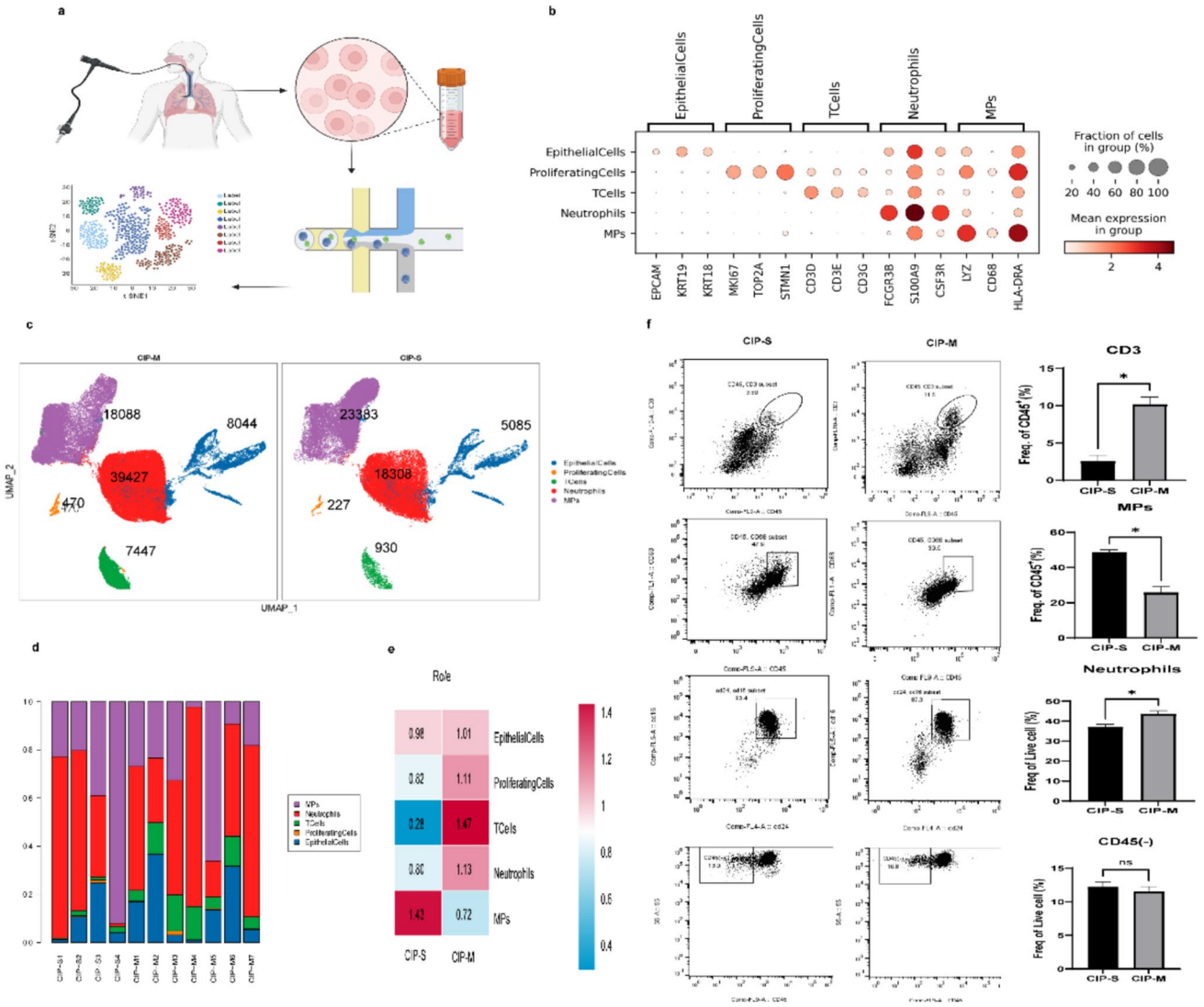

Fig. 1 Main cell type of immune checkpoint inhibitor-related pneumonitis in BALF. **a** The flowchart illustrating the procedure of gathering Bronchoalveolar Lavage Fluid (BALF) to conduct single-cell sequencing analysis. **b** Five major cell type annotation of 121,409 high qualified BALF cells. **c** UMAP presentation of the main cell types (Epithelial cells, Proliferating cells, T cells, Neutrophils, MPs (Mononuclear phagocytes)) in CIP-S and CIP-M group. **d** Relative proportions of main cell types identified on each patient. **e** The Ro/e (Observed to Expected Ratio) method was employed to compare the relative cell type abundance between the CIP-S and CIP-M groups. (Ro/e > 1 signifying enrichment in the group.). **f** CD3, MPs, Neutrophils and CD45 negative cells (Epithelial cells and Proliferating cells) were detected by Flow cytometry between CIP-S and CIP-M group. ($n = 4$, P-value was assessed by Mann–Whitney U test)

one used Durvalumab, one used Tislelizumab and one had a history of thoracic radiotherapy. In the CIP-M group, six patients were diagnosed with lung cancer, one was gastric cancer, five patients smoked, four had thoracic radiotherapy history, two received Pembrolizumab, three received Toripalimab, one received Duralumab, and one received Tislelizumab treatment (Table 1). The median time from treatment to CIP was 249.5 days in CIP-S group and 290.4 days in CIP-M group. The median overall survival time was 58.5 days in CIP-S group, while not reached for CIP-M group. After quality control, we obtained a total of 121,409 high-quality cells. Through clustering and visualization, we annotated five cell types, including epithelial cells (EPCAM, KRT19, KRT18), proliferating cells (MKI67, TOP2A, STMN1), T cells (CD3E, CD3E, CD3G), neutrophils (FCGR3B, S100A9, CSF3R), and mononuclear phagocytes (LYZ, CD68, HLA-DRA) according to their canonical gene markers (Fig. 1b). All the cases had these five clusters. Ro/e method was used to compare the distribution of cells between two groups (Fig. 1e). It was found that the CIP-S group had a higher percentage of mononuclear phagocytic system (MPs) cells, while the CIP-M group had a higher percentage of T cells and neutrophils (Fig. 1c). Flow cytometry validation analysis supported the above results (Fig. 1f).

Epithelial cell landscape in the BALF of different grades of CIP patients

A total of 13,129 epithelial cells were annotated, and then reclustered and identified into five clusters. AlveolarEpi (SFTPC, SFTPB, NAPSA), ciliated cells (C20orf85, RSPH1, SNTN), ionocytes (CEL, ASCL3, STAP1), secretory cells (SCGB1A1, SCGB3A1, MSMB), squamous cells (SPRR3, MAL, KRT13), and aberrant basaloid cells (MIEN1, MMP7, ERBB2) (Fig. 2a). In the CIP-S group, aberrant basaloid and AlveolarEpi cells accounted for a higher percentage, whereas ciliated cells and secretory cells predominate in the CIP-M group (Fig. 2b and e). To our knowledge, this is the first study to report aberrant basaloid cells in the BALF of CIP. CNV analysis revealed that aberrant basaloid cells have a higher copy number of variants (Fig. 2c and d). Compared with other epithelial cells, aberrant basaloid cells exhibited a significantly larger number of differentiated genes, both upregulated and downregulated (Fig. 2f). The results of flow cytometry verified the significant enrichment of aberrant basaloid cells in CIP-S group (Fig. 2g). We performed GO analysis on the differences in highly expressed genes between CIP-S and CIP-M. Results showed enrichment of MHC class II pathway in CIP-S group. Comparing MHC- II expression with UCell method in we found that CIP-S group had higher MHC- II expression score than CIP-M (Fig S2a, Table S2). GSEA analysis between aberrant basaloid cells and the other epithelial cells showed that neutrophil chemotaxis and the activity of chemokines and cytokines were raised in aberrant basaloid cells (Fig. 2h). CXCL3, CXCL5, and CXCL8 in the neutrophil chemotaxis pathway had indeed higher scores in aberrant basaloid cells than in other epithelial cells (Fig. S2b-d). All of these findings indicate that aberrant basaloid cells may secrete more chemokines and cytokines, featuring robust antigen presentation and activation of the immune system. We conducted further analysis on the transcription factor regulatory network of aberrant basaloid cells. SOX9, ZNF281, JUN, KLF6 and ELF4 were the top 5 regulons (pySCENIC) (Fig. 2i). We analyzed the target genes of these transcription factors, and discovered that CXCL3, and CXCL5 were highly ranked targets of SOX9, with CXCL3 in particular positioned as the second most important gene (Table S1). Whereafter, pathway enrichment analysis on the target genes of SOX9 showed that the molecular functions of these genes were primarily focused on CXCR chemokine receptor binding and chemokine activity (Fig. S2f).

Characteristics of neutrophils in BALF of different grades of CIP patients

Reclustering of neutrophils resulted in the identification of four distinct subclusters, which were labeled as Neutrophils_CXCR2, Neutrophils_CCL3, Neutrophils_MMP9, and Neutrophils_ISG15 based on their top three DEGs (Fig. 3a). Compared with CIP-M group, Neutrophils in the CIP-S group showed more enrichment of immune activation-related pathways, such as the Toll-like receptor signaling pathway and leukocyte chemotaxis (Fig. 3b and c). Furthermore, Neutrophil_CXCR2 subcluster in CIP-S group was related to T cell activation, chemokine signaling pathway and leukocyte transendothelial migration (Fig. 3d and e). Then Gene set scoring showed that Neutrophils in the CIP-S group have a higher score of antigen presentation and pro-inflammatory signatures and a lower score of pro-angiogenic signature (Fig. 3f–h, Table S2). Further, we analyzed the peripheral blood routine parameters of patients at the time of BALF collection. Percentage and absolute value of neutrophils in the CIP-S group were higher than those in the CIP-M group, while the percentage of lymphocytes in the CIP-S group was elevated, but there was no significant difference in their absolute values (Fig. 3i–l).

T cell subtypes and differential gene set enrichment analysis on different grades of CIP patients

Further analysis of T cells annotated 4 clusters: NK (TRDC, KLRF1, TYROBP), CD4 NaiveT (CCR7, LTB, IL7R), CD4 Treg (IL2RA, MAF, TNFRSF4), and CD8 Teff (CD8A, CD8B, TRGC2) cells (Fig. 4a). CD8 Teff and CD4 Treg were enriched in CIP-S group, while NK and CD4 Naive T

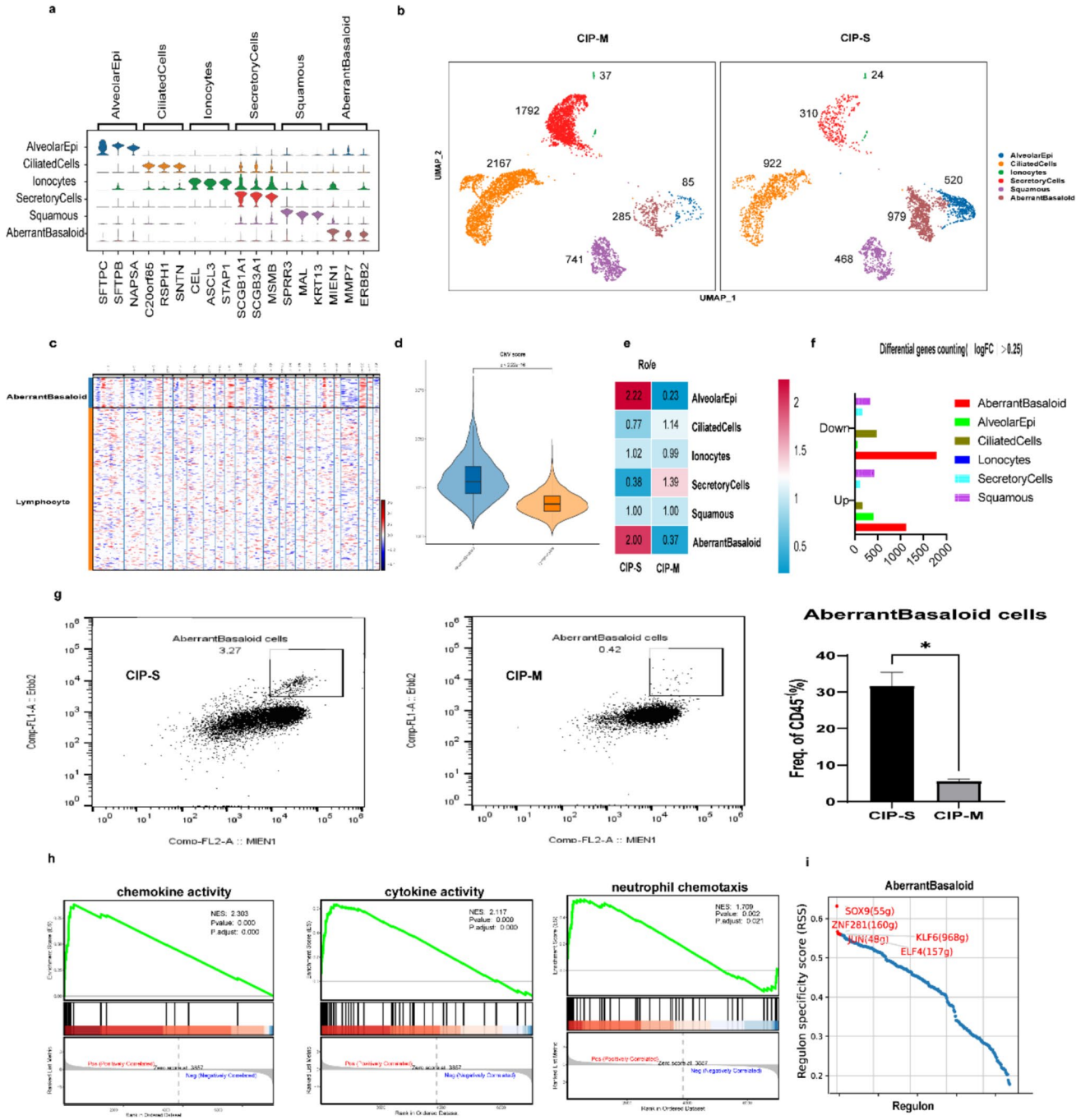

Fig. 2 Aberrant basaloid cells were enriched in the BALF of CIP-S patients, potentially activating neutrophils. **a** Epithelial cells were sub-clustered into six clusters according to canonical marker gene expression. **b** UMAP presentation showed aberrant basaloid cells and AlveolarEpi cells were enriched in CIP-S groups. **c/d** CNV analysis revealed aberrant basaloid cells had a higher copy number of variants. **e** Ro/e meathod was employed to compare the relative abundance between CIP-S and CIP-M group. **f** Aberrant basaloid cells had the highest number of differentially expressed genes between the CIP-S and CIP-M groups. (|logFC|> 0.25) **g** Flow cytometry analysis indicated CIP-S group was enriched with aberrant basaloid cells (Marked by MMP7, MIEN1 and ERBB2, flow cytometry plot shows the MIEN1^{+} and ERBB2^{+} cells' proportion of MMP7^{+} cells. And statistical analysis shows the proportion of aberrant basaloid cells in CD45 negative cells), **h** GSEA analysis between aberrant basaloid cells and the other epithelial cells found that neutrophil chemotaxis, the activity of chemokines and cytokines are raised in aberrant basaloid cells. **i** Transcription factor network was constructed (pySCENIC V0.11.0) between aberrant basaloid cells and the other epithelial cells. And SOX9, ZNF281, JUN, KLF6 and ELF4 were the top 5 regulon

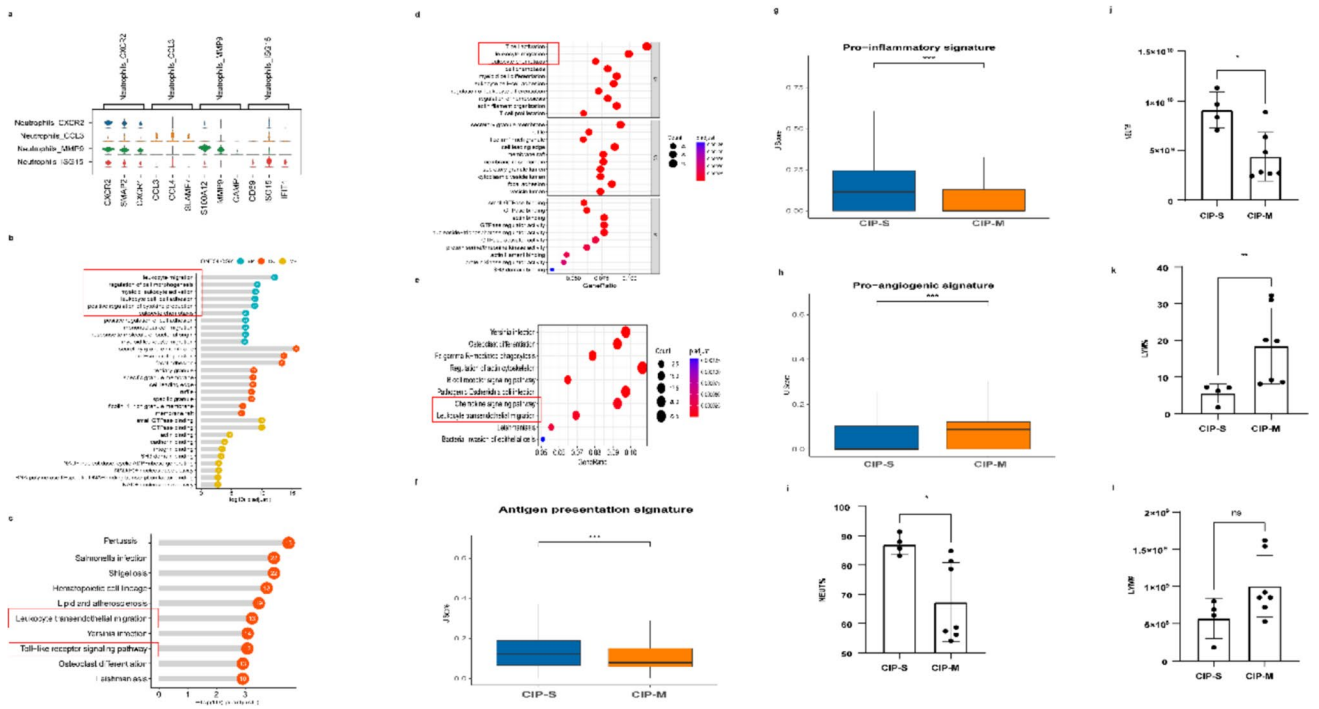

Fig. 3 Neutrophils were activated in the BALF of severe CIP patients. **a** Neutrophils were sub-clustered into four clusters. **b/c** GO and KEGG analysis showed neutrophils in the CIP-S group were enriched in immune activation-related pathways, such as the Toll-like receptor signaling pathway, leukocyte chemotaxis. **d/e** Further analysis showed that neutrophil_CXCR2 subcluster in CIP-S group was related to T cell activation, chemokine signaling pathway and leukocyte transendothelial migration. **f–h** Gene set scoring showed neutrophils in the CIP-S group have a higher score of antigen presentation signature and pro-inflammatory and lower score of Pro-angiogenic signature. **I–l**. Percentage and absolute value of peripheral neutrophils in the CIP-S group were higher than those in the CIP-M group, while the percentage of lymphocytes in the CIP-S group was elevated, but there was no statistical significance for their absolute values

were enriched in CIP-M group (Fig. 4b–d). Flow cytometry verified the significant enrichment of CD8 T cells in the CIP-S group (Fig. 2h). GO analysis showed that upregulated genes in CIP-S group were enriched in T cell activation and antigen processing (Fig. 4e). Similarly, KEGG revealed enrichment of antigen processing and presentation signaling pathways. Therefore, T cells should be more active in the CIP-S group (Fig. 4f).

MPs subtypes and differential gene set enrichment analysis on different grades of CIP patients

MPs were further annotated as mast cells (TPSAB1, CPA3, TPSB2), macrophages (CD68, C1QA, C1QB), and monocytes (CD14, LYZ, FCN1) (Fig. 5a). Macrophages were the main population of MPs and seemed to be more enriched in the CIP-S group, while Monocytes were concentrated in the CIP-M group (Fig. 5b–d). GO analysis of upregulated genes in macrophages of the CIP-S group showed macrophage activation, T cell activation, leukocyte migration, and antigen processing and presentation (Fig. 5e and f).

Cell communications between aberrant basaloid and immune cells

To determine whether communications exist between aberrant basaloid and immune cells, we analyzed the ligand-receptor interaction using Cellchat and CellPhone DB. We found that CD8 T cells and neutrophils were the top two immune cells that interact intensely with aberrant basaloid cells (Fig. 6a). According to information flow, the chemokine pathways increased more obviously in the CIP-S group than in the CIP-M group (Fig. 6e). Further, UCell scoring was performed on the CXCL pathway of aberrant basaloid cells and neutrophils (Table S2). The statistical results showed that the CXCL pathway was indeed more enriched in the CIP-S group than in the CIP-M group (Fig. 6c). Heatmap of the CXCL signaling pathway network demonstrated that aberrant basaloid cells were the sender and neutrophils were both the mediator and the receiver (Fig. 6e). CellPhoneDB revealed that CXCL1/2/3/5/8-CXCR2 and CXCL8-CXCR1 were the top ligand-receptor pairs for chemokines (Fig. 6d).

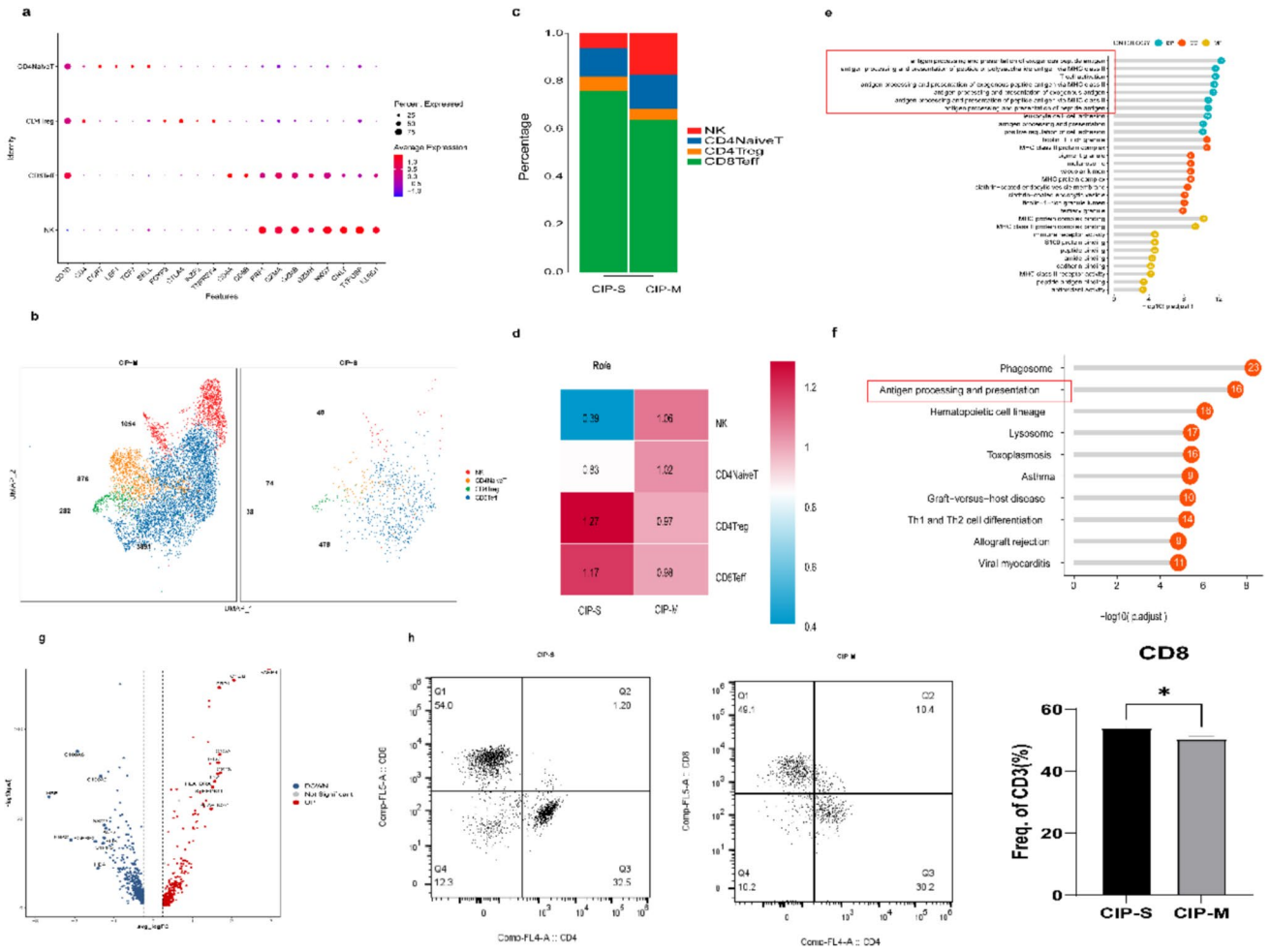

Fig. 4 T cell landscape in the BALF of different grade of CIP patients. **a** T cells were sub-clustered into four clusters according to canonical marker gene expression. **b–d** Relative proportions, UMAP presentation and Ro/e analysis showed $CD8^{+}$T effective cells were enriched in CIP-S group. **e/f** GO and KEGG analysis of upregulated genes of T cells in the CIP-S group revealed that T cell activation and antigen processing and presentation were the most significant processes. **g** Volcano plot shows the differentially expressed genes between the CIP-S and CIP-M groups. (|logFC|> 0.25). **h** Flow cytometry validates the above results ($n=4$, P value was assessed by Mann–Whitney *U* test)

Based on the above findings, we deduced that aberrant basaloid cells increased in CIP-S patients' BALF, which highly expressed SOX9 and increased CXCL3/5 expression, and then interacted with the CXCR2 receptors on neutrophils, leading to the activation of the patients' immune system.

Discussion

CIP is one of the common irAEs, and also the leading cause of patient death related to PD-1/PD-L1 antibodies [25, 32, 33, 36]. Interestingly, despite the relatively low incidence of CIP in clinical trials, which is around 5%, the actual data from the real world suggest that the incidence of CIP could be as high as 20%, and the percentage of patients with severe pneumonia is quite significant [4, 15, 16, 28]. Therefore, analyzing the pathogenesis of various levels of CIP is of great clinical significance. Here we focus on the pneumonitis after the immunotherapy, whatever the cancer type. Although, the biases of cancer types and sex in the cohort could be an impact. But it was really difficult to collect enough samples. In previous studies, comparative research was mainly conducted between patients who developed CIP and those who did not. For example, Karthilk Suresh et al. indicated that there was an increase in CD4 T cells and central memory T cells in the bronchoalveolar lavage fluid (BALF) of CIP patients [32, 33]. Franken and Pengfei Cui et al. suggested that monocytes with pro-inflammatory effects were enriched in CIP [7, 13]. It is known that the clinical outcomes for severe and mild CIP patients can be markedly different, with severe cases often resulting in

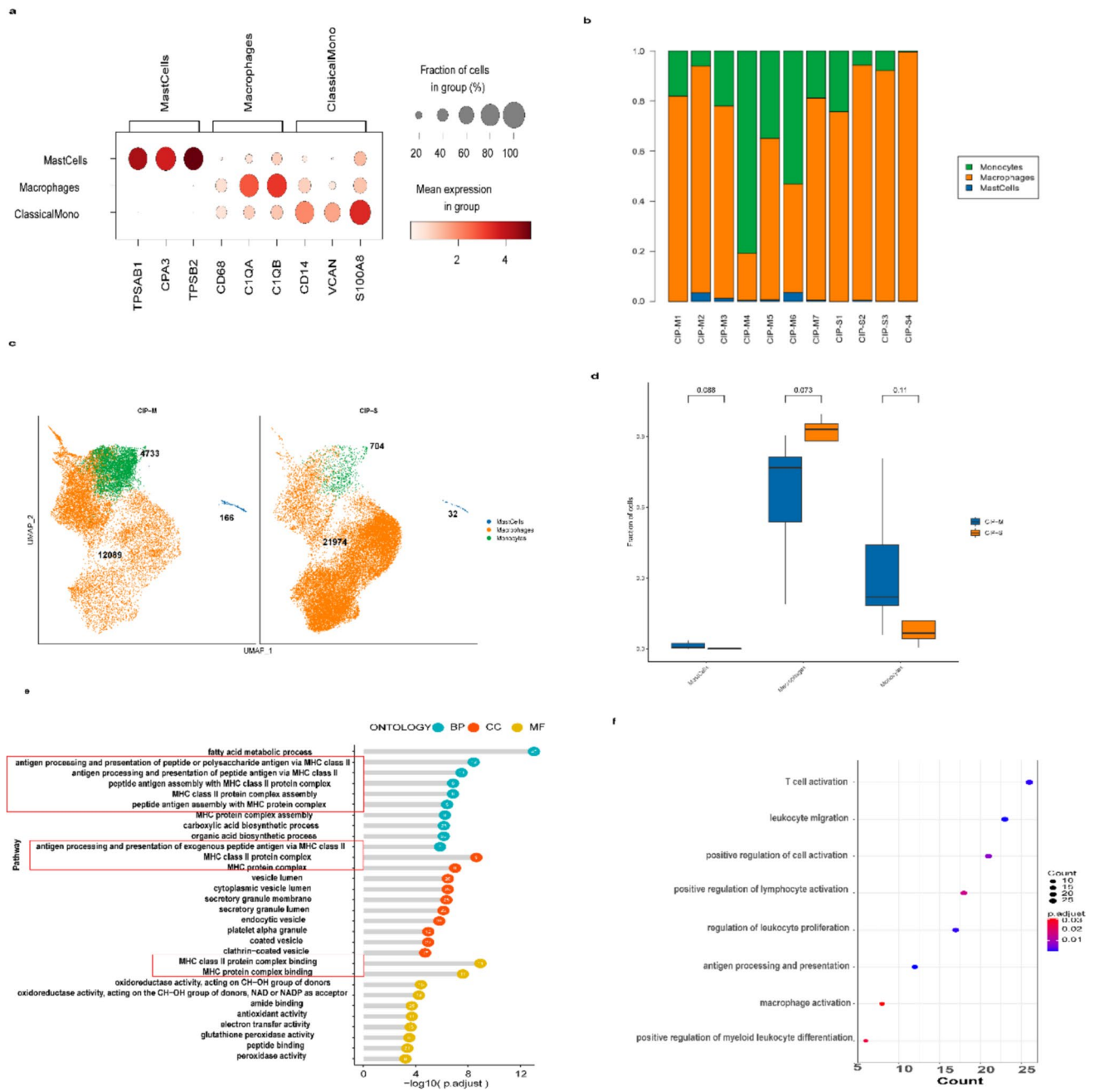

Fig. 5 Mononuclear phagocytic system landscape in the BALF of different grade of CIP patients. **a** Mononuclear phagocytic system was sub-clustered into Macrophages, mast cells and Classical monocytes according to canonical marker gene expression **b/d** Relative proportions of each patient and relative abundancy between groups using Wilcoxon rank-sum test. **c** Macrophages tended to be enriched in the CIP-S group, whereas mast cells and classical monocytes seemed to be enriched in the CIP-M group. **e/f** GO analysis of upregulated genes in macrophage of CIP-S group showed macrophage activation, T cell activation, leukocyte migration, antigen processing and presentation

fatal outcomes. To our knowledge, our study is the first to explore the differences in the immune microenvironments of BALF between severe and mild CIP patients. This approach may provide valuable insights into the mechanisms of CIP and directions for future research. In the current study, we identified a population of epithelial cells enriched in CIP-S patients, named aberrant basaloid cells, highly expressing MIEN1, MMP7 and ERBB2 (Fig. S1). Aberrant basaloid cells were first reported in idiopathic pulmonary fibrosis, co-expressing basal epithelial, mesenchymal, senescence, and developmental markers [1]. In our study, aberrant basaloid cells significantly expressed MIEN1 and MMP7,

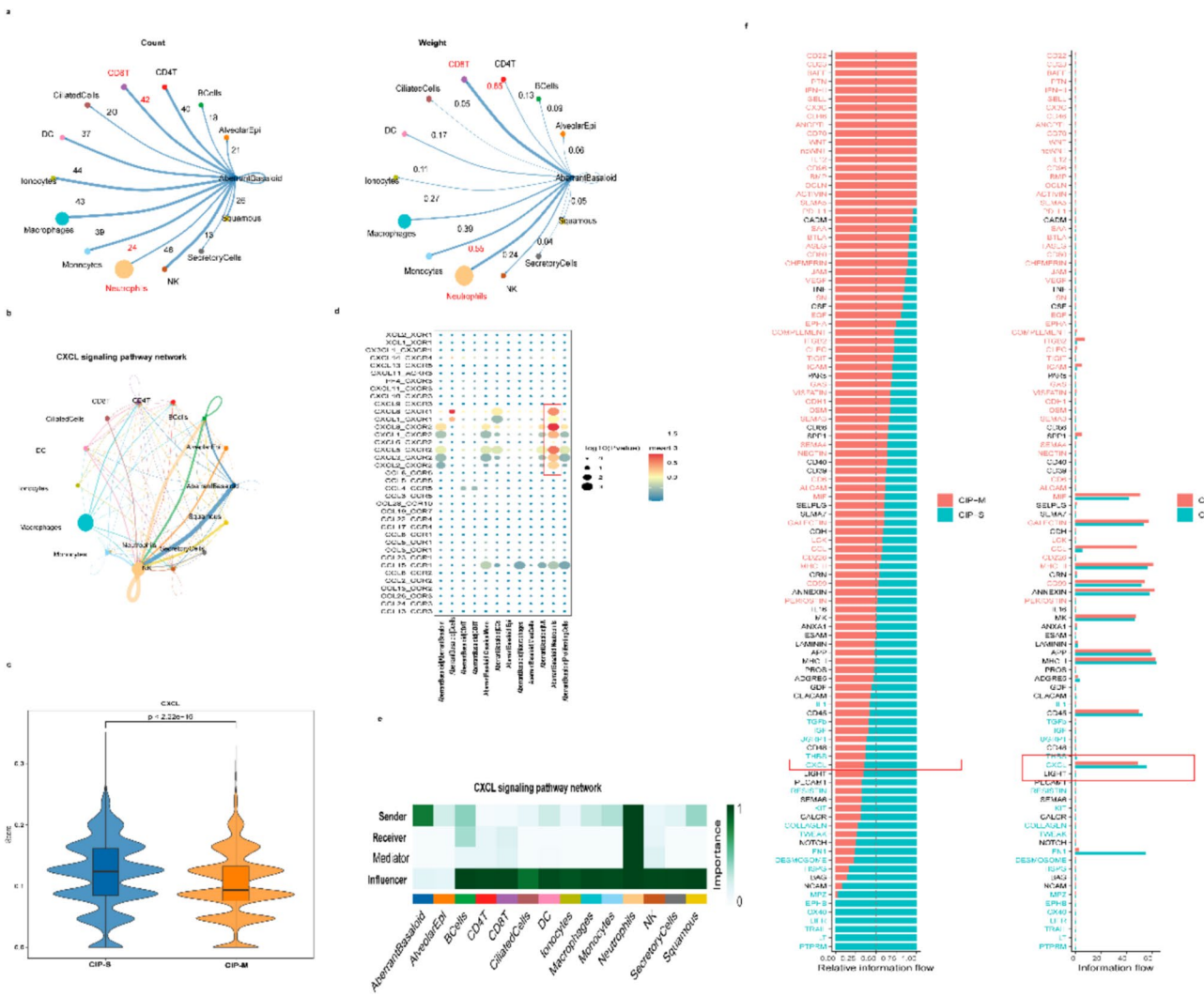

Fig. 6 Cell communications between epithelial cells and immune cells. **a** Ligand-receptor interactions analysis by using Cellchat showed CD8T cells and neutrophils were the top two immune cells that interact intensely with aberrant basaloid cells. (Thickness of the lines represents the intensity of the interaction between cells, and the size of the circles represents the number of interacting cells). **b** Further analysis showed CXCL signaling pathway was the major crosstalk pathway between aberrant basaloid cells and neutrophils. **c** CXCL pathway of aberrant basaloid cells and neutrophils scored by UCell method. (*P* value was assessed by Wilcoxon rank-sum test) **d** CellPhone DB results showed that CXCL1/2/3/5/8CXCR2 and CXCL8-CXCR1 were the top ligand-receptor pairs of chemokines. **e** Aberrant basaloid cells were the sender and neutrophils were the receiver. **f** Information flow showed chemokine pathway in the CIP-S group was stronger increased than that in the CIP-M group

which were related to epithelial-mesenchymal transition (EMT). The protein encoded by the MIEN1 gene is related to the migration and invasion abilities of epithelial cells [21]. In damaged lung epithelial cells, MMP7 functions as an inducer of syndecan-1 shedding, carrying CXCL1 on its glycosaminoglycan chain. This leads to the release of the syndecan-1-CXCL1 complex, which is essential for the intrapulmonary infiltration of neutrophils. MMP7 involvement in neutrophil infiltration promotes epithelial cell damage and fibrosis [23]. SOX9 as a transcription factor plays a crucial role in cellular differentiation and development, and functions in a variety of physiological processes, including sex determination, chondrocyte differentiation, and maintenance of stem cell stability(Du G et al., 2024; [27, 30]). In addition, SOX9 has recently been reported to play a vital role in the formation and development of alveolar epithelium, not only guiding the differentiation of stem cells but affecting the early structural development of the alveoli. SOX9-positive stem cells also exert a significant effect on lung regeneration [2, 40]. We speculate that during the onset of CIP-S, alveolar epithelial injury triggers the upregulation of SOX9, in turn leading to the differentiation of an aberrant population of basal cells. In this study, these cells are designated as aberrant

basaloid cells. Meanwhile, SOX9 upregulates the expression of chemokines such as CXCL3, and 5, which subsequently bind to the CXCR2 receptor on neutrophils, promoting their migration and activation. These findings suggest that blocking SOX9 upregulation, chemokine secretion, or neutrophil binding may potentially prevent CIP-S.

Limitation

This study has several limitations. First, the collection of BALF from patients with CIP is difficult, especially from CIP-S patient, thus limiting the sample size. Our research is still ongoing, and future analysis may enlarge the sample size to verify the current results. Second, these results are based on transcriptome sequencing, and mechanistic studies showing that aberrant basaloid cells are causal to tissue damage in severe CIP animal experiments are required for further validation. But no standard animal model is available for CIP. Finally, not all the cases in this study used PD-1 antibody, and it has been reported that the incidence of CIP or CIP-S is lower when using PD-L1 antibody than other ICIs [19]. The mechanisms of CIP may not be the same among different types of ICIs including PD-1, PD-L1 and CTLA-4 antibodies.

Supplementary Information The online version contains supplementary material available at https://doi.org/10.1007/s00262-025-03983-8.

Acknowledgements We thank all the patients involved in this study. We also thank support from the Technology Innovation and Application Development Project of Chongqing (2023DBXM002, CSTB2022TIAD-KPX0176), the National Natural Science Foundation of China (82172670 and 82473261), the Leading medical talents of Chongqing (YXLJ202401), Noncommunicable Chronic Diseases-National Science and Technology Major Project (2023ZD0502105).

Author contributions Jianguo Sun designed the study and approved the final manuscript for publication. Linpeng Zheng analyzed the results and wrote the manuscript. Dingqin Cai and Jianbo Zhu enrolled patients (Table 1). Fenglin Lin, Longyao Zhang, Chenrui Yin, Yaxian, Qi and Lingyou Sun collected the BALF samples (Table 1 and Fig. 1). Lingchen Li and Xiewan Chen drew the figures and modified the manuscript (Fig. 1, Fig. 2, Fig. 3, Fig. 4, Fig. 5, and Fig. 6). Authors have given their consent to the submission of the manuscript and have thoroughly reviewed and endorsed the final draft. Furthermore, they collectively assume full accountability for the manuscript's content, ensuring the precision of the data and the accuracy of its statistical analysis.

Funding This study was supported by the Technology Innovation and Application Development Project of Chongqing (2023DBXM002, CSTB2022TIAD-KPX0176)), the National Natural Science Foundation of China (82172670 and 82473261), the Leading medical talents of Chongqing (YXLJ202401), Noncommunicable Chronic Diseases-National Science and Technology Major Project (2023ZD0502105).

Data availability No datasets were generated or analyzed during the current study.

Declarations

Conflict of interest The authors declare no competing interests.

Consent for publication All the authors approved the publication of the manuscript.

Ethical approval This study had been registered at ClinicalTrials.gov. (NCT05455034) and received ethical approval from the hospital (NO. 2022–022-01).

References

1. Adams TS, Schupp JC, Poli S et al (2020) Single-cell RNA-seq reveals ectopic and aberrant lung-resident cell populations in idiopathic pulmonary fibrosis. SCI ADV 6:a1983
2. Alysandratos KD, Herriges MJ, Kotton DN (2021) Epithelial stem and progenitor cells in lung repair and regeneration. ANNU REV PHYSIOL 83:529–550
3. Andreatta M, Carmona SJ (2021) UCell: Robust and scalable single-cell gene signature scoring. Comput Struct Biotechnol J 19:3796–3798
4. Atchley WT, Alvarez C, Saxena-Beem S et al (2021) Immune checkpoint inhibitor-related pneumonitis in lung cancer: real-world incidence, risk factors, and management practices across six health care centers in North Carolina. Chest 160:731–742
5. Chang SH, Mirabolfathinejad SG, Katta H et al (2014) T helper 17 cells play a critical pathogenic role in lung cancer. Proc Natl Acad Sci U S A 111:5664–5669
6. Chen S, Kang Y, Li D et al (2022) Diagnostic performance of metagenomic next-generation sequencing for the detection of pathogens in bronchoalveolar lavage fluid in patients with pulmonary infections: systematic review and meta-analysis. INT J INFECT DIS 122:867–873
7. Cui P, Li J, Tao H et al (2023) Deciphering pathogenic cellular module at single-cell resolution in checkpoint inhibitor-related pneumonitis. Oncogene 42:3098–3112
8. Dobin A, Davis CA, Schlesinger F et al (2013) STAR: ultrafast universal RNA-seq aligner. Bioinformatics 29:15–21
9. Du G, Zhang J, Shuai Q et al (2024) Development of alginate-collagen interpenetrating network for osteoarthritic cartilage by in situ softening. Int J Biol Macromol 266:131259
10. Dura B, Choi JY, Zhang K et al (2019) scFTD-seq: freeze-thaw lysis based, portable approach toward highly distributed single-cell 3' mRNA profiling. Nucleic Acids Res 47:e16

11. Emens LA, Romero PJ, Anderson AC et al (2024) Challenges and opportunities in cancer immunotherapy: a Society for Immunotherapy of Cancer (SITC) strategic vision. J Immunother Cancer 12:009063
12. Fehrenbacher L, Spira A, Ballinger M et al (2016) Atezolizumab versus docetaxel for patients with previously treated non-small-cell lung cancer (POPLAR): a multicentre, open-label, phase 2 randomised controlled trial. Lancet 387:1837–1846
13. Franken A, Van Mol P, Vanmassenhove S et al (2022) Single-cell transcriptomics identifies pathogenic T-helper 17.1 cells and pro-inflammatory monocytes in immune checkpoint inhibitor-related pneumonitis. J Immunother Cancer 10:005323
14. Gettinger SN, Horn L, Gandhi L et al (2015) Overall survival and long-term safety of Nivolumab (anti-programmed death 1 antibody, BMS-936558, ONO-4538) in patients with previously treated advanced non-small-cell lung cancer. J Clin Oncol 33:2004–2012
15. Guo C, Zhang Q, Zhou P et al (2024) The application of bronchoscopy in the assessment of immune checkpoint inhibitor-related pneumonitis severity and recurrence. Sci Rep 14:17137
16. Herbst RS, Baas P, Kim DW et al (2016) Pembrolizumab versus docetaxel for previously treated, PD-L1-positive, advanced non-small-cell lung cancer (KEYNOTE-010): a randomised controlled trial. Lancet 387:1540–1550
17. Jin S, Guerrero-Juarez CF, Zhang L et al (2021) Inference and analysis of cell-cell communication using cell chat. Nat Commun 12:1088
18. Jovic D, Liang X, Zeng H et al (2022) Single-cell RNA sequencing technologies and applications: a brief overview. Clin Transl Med 12:e694
19. Khunger M, Rakshit S, Pasupuleti V et al (2017) Incidence of pneumonitis with use of programmed death 1 and programmed death-ligand 1 inhibitors in non-small cell lung cancer: a systematic review and meta-analysis of trials. Chest 152:271–281
20. Kim ST, Sheshadri A, Shannon V et al (2020) Distinct immunophenotypes of T cells in bronchoalveolar lavage fluid from leukemia patients with immune checkpoint inhibitors-related pulmonary complications. Front Immunol 11:590494
21. Kushwaha PP, Gupta S, Singh AK et al (2019) Emerging role of migration and invasion enhancer 1 (MIEN1) in cancer progression and metastasis. Front Oncol 9:868
22. Liao Y, Smyth GK, Shi W (2014) featureCounts: an efficient general purpose program for assigning sequence reads to genomic features. Bioinformatics 30:923–930
23. Mahalanobish S, Saha S, Dutta S et al (2020) Matrix metalloproteinase: an upcoming therapeutic approach for idiopathic pulmonary fibrosis. Pharmacol Res 152:104591
24. Mountzios G, Remon J, Hendriks L et al (2023) Immune-checkpoint inhibition for resectable non-small-cell lung cancer - opportunities and challenges. Nat Rev Clin Oncol 20:664–677
25. Naidoo J, Wang X, Woo KM et al (2017) Pneumonitis in patients treated with anti-programmed death-1/programmed death ligand 1 therapy. J Clin Oncol 35:709–717
26. Papalexi E, Satija R (2018) Single-cell RNA sequencing to explore immune cell heterogeneity. Nat Rev Immunol 18:35–45
27. Qian G, Yu Y, Dong Y et al (2024) Exosomes derived from human urine-derived stem cells ameliorate IL-1beta-induced intervertebral disk degeneration. BMC Musculoskelet Disord 25:537
28. Reck M, Rodriguez-Abreu D, Robinson AG et al (2016) Pembrolizumab versus chemotherapy for PD-L1-positive non-small-cell lung cancer. N Engl J Med 375:1823–1833
29. Stachowiak Z, Narozna B, Szczepankiewicz A (2023) Non-coding RNAs in pulmonary diseases: comparison of different airway-derived biosamples. INT J MOL SC I:24
30. Su H, Yan Q, Du W et al (2024) Calycosin ameliorates osteoarthritis by regulating the imbalance between chondrocyte synthesis and catabolism. BMC Complement Med Ther 24:48
31. Subramanian A, Tamayo P, Mootha VK et al (2005) Gene set enrichment analysis: a knowledge-based approach for interpreting genome-wide expression profiles. Proc Natl Acad Sci U S A 102:15545–15550
32. Suresh K, Naidoo J, Zhong Q et al (2019) The alveolar immune cell landscape is dysregulated in checkpoint inhibitor pneumonitis. J CLIN INVEST 129:4305–4315
33. Suresh K, Psoter KJ, Voong KR et al (2019) Impact of checkpoint inhibitor pneumonitis on survival in NSCLC patients receiving immune checkpoint immunotherapy. J Thorac Oncol 14:494–502
34. Tanaka Y, Nakai T, Suzuki A et al (2023) Clinicopathological significance of peritumoral alveolar macrophages in patients with resected early-stage lung squamous cell carcinoma. Cancer Immunol Immunother 72:2205–2215
35. Tirosh I, Venteicher AS, Hebert C et al (2016) Single-cell RNA-seq supports a developmental hierarchy in human oligodendroglioma. Nature 539:309–313
36. Wang DY, Salem JE, Cohen JV et al (2018) Fatal toxic effects associated with immune checkpoint inhibitors: a systematic review and meta-analysis. JAMA Oncol 4:1721–1728
37. Wolf FA, Angerer P, Theis FJ (2018) SCANPY: large-scale single-cell gene expression data analysis. Genome Biol 19:15
38. Yu G, Wang LG, Han Y et al (2012) clusterProfiler: an R package for comparing biological themes among gene clusters. OMICS 16:284–287
39. Zhang H, Deng D, Li S et al (2023) Bronchoalveolar lavage fluid assessment facilitates precision medicine for lung cancer. Cancer Biol Med 21:230–251
40. Zhang K, Yao E, Chuang E et al (2022) mTORC1 signaling facilitates differential stem cell differentiation to shape the developing murine lung and is associated with mitochondrial capacity. Nat Commun 13:7252
41. Zhang L, Yu X, Zheng L et al (2018) Lineage tracking reveals dynamic relationships of T cells in colorectal cancer. Nature 564:268–272
42. Zhang N, Yang X, Piao M et al (2024) Biomarkers and prognostic factors of PD-1/PD-L1 inhibitor-based therapy in patients with advanced hepatocellular carcinoma. Biomark Res 12:26
43. Zhang X, Zhu R, Yu D et al (2024) Single-cell RNA sequencing to explore cancer-associated fibroblasts heterogeneity: "Single" vision for "heterogeneous" environment. Cell Prolif 57:e13592